Smart Structures and Systems, *Vol. 27, No. 2 (2021) 351-363*
DOI: https://doi.org/10.12989/sss.2021.27.2.351

Clump interpolation error for the identification of damage using decentralized sensor networks

Said Quqa*[1], Pier Francesco Giordano[2a], Maria Pina Limongelli[2b], Luca Landi[1c] and Pier Paolo Diotallevi[1d]

[1] *Department DICAM, Università di Bologna, Viale del Risorgimento 2, 40136 Bologna, Italy*
[2] *Department ABC, Politecnico di Milano, Piazza Leonardo Da Vinci 32, 20133 Milan, Italy*

(*Received June 6, 2020, Revised September 9, 2020, Accepted October 2, 2020*)

Abstract. Recent developments in the field of smart sensing systems enable performing simple onboard operations which are increasingly used for the decentralization of complex procedures in the context of vibration-based structural health monitoring (SHM). Vibration data collected by multiple sensors are traditionally used to identify damage-sensitive features (DSFs) in a centralized topology. However, dealing with large infrastructures and wireless systems may be challenging due to their limited transmission range and to the energy consumption that increases with the complexity of the sensing network. Local DSFs based on data collected in the vicinity of inspection locations are the key to overcome geometric limits and easily design scalable wireless sensing systems. Furthermore, the onboard pre-processing of the raw data is necessary to reduce the transmission rate and improve the overall efficiency of the network. In this study, an effective method for real-time modal identification is used together with a local approximation of a damage feature, the interpolation error, to detect and localize damage due to a loss of stiffness. The DSF is evaluated using the responses recorded at small groups of sensors organized in a decentralized topology. This enables the onboard damage identification in real time thereby reducing computational effort and memory allocation requirements. Experimental tests conducted using real data confirm the robustness of the proposed method and the potential of its implementation onboard decentralized sensor networks.

Keywords: instantaneous modal parameter; damage identification; interpolation error; filter bank; cluster

1. Introduction

Due to the significant amount of data necessary to perform damage identification analyses using traditional techniques, the majority of continuous monitoring systems deployed on civil structures are wired and data are generally analyzed offline, after collection (Kaya and Safak 2015). However, in large infrastructures, cables and data acquisition systems may involve a considerable increase in costs, also considering the fact that specific low-noise cables should be used to cover long distances. Furthermore, physical obstacles may hinder cable deployment, making the design of the acquisition system even more challenging. Relevant studies have demonstrated the effectiveness of wireless smart sensor networks (WSSNs) for Structural Health Monitoring (SHM) applications (Jang *et al*. 2010, Rice *et al*. 2010) nonetheless highlighting these limitations for large networks of sensors organized in complex topologies, which may affect the efficiency of battery-powered devices. Decentralization has shown to be a solution to these issues, limiting data transmissions thanks to onboard compression procedures. Groundbreaking studies were conducted extending traditional techniques, such as the damage locating vector (DLV) (Gao *et al*. 2006, Nagayama *et al*. 2009), to allow their application in a decentralized fashion. More recently, methods based on time-series representations (Long and Büyüköztürk 2017) and artificial neural networks (ANNs) (Avci *et al*. 2018) have been proposed as promising alternatives thanks to the small amount of data necessary to evaluate the Damage-Sensitive Features (DSFs).

In this paper, the use of the Interpolation Method (IM) as a DSF using decentralized WSSNs is investigated. In the original formulation of the method, the DSF is evaluated using the data collected through all the acquisition channels. However, due to the characteristics of the cubic spline function used for the interpolation, at each sensor location, the value of the DSF mainly depends on the responses recorded by a small subset of neighboring sensors. The suitability of using subsets of sensors for the evaluation of the IM is investigated in this work, analyzing different sensor topologies. Two important aspects to tackle in the application of the IM are the identification of the modal amplitudes and the choice of the boundary conditions at the ends of the interpolation range which, in this case, coincides with the subset of sensors used for the interpolation.

*Corresponding author, Ph.D. Fellow,
E-mail: said.quqa2@unibo.it
[a] Ph.D. Fellow, E-mail: pierfrancesco.giordano@polimi.it
[b] Associate Professor, E-mail;
mariagiuseppina.limongelli@polimi.it
[c] Associate Professor, E-mail: l.landi@unibo.it
[d] Professor, E-mail: pierpaolo.diotallevi@unibo.it

http://www.techno-press.org/?journal=sss&subpage=7
ISSN: 1738-1584 (Print), 1738-1991 (Online)

Regarding the first aspect, it is important to note that civil structures usually do not fulfill the stationarity assumptions at the base of most identification algorithms used for vibration-based SHM. This is the case of bridges under non-stationary excitation due to traffic or railway loads (Li *et al*. 2003, Pakrashi *et al*. 2010, Spiridonakos and Fassois 2009). Non-stationarities are usually neglected in traditional identification methods, that consider wide signal windows to evaluate averaged dynamic parameters. This increases the robustness of the SHM process but may lead to unreliable outcomes in the health assessment process. Furthermore, in order to study the variability in time of structural features, to find possible correlations with other measurements (e.g., temperature, loads, and strong excitation) and discern actual damage from operational and environmental effects (Kaya and Safak 2015) or also to reliably detect damage which may appear only under certain conditions (Nguyen 2013), the instantaneous identification of dynamic parameters is crucial. In the last years, thanks to the growing interdisciplinarity among the fields of signal processing and structural dynamics (Brincker and Ventura 2015), an increasing number of algorithms for instantaneous identification of modal features have been proposed. Linear algebra and subband coding have been exploited to envision robust "DSFs" based upon time-frequency and time-scale representations of nonstationary signals (Vetterli and Kovačević 1995). The short-time Fourier transform (STFT) (Gabor 1946) and the wavelet transform (WT) (Daubechies 1992) are among the most used linear transforms in the field of SHM, the first employing a fixed complex exponential kernel function, while the second relying on a family of more flexible functions for the signal decomposition. Several researchers (Kijewski and Kareem 2003, Nagarajaiah and Basu 2009) demonstrated the suitability of these techniques for modal identification in output-only conditions. More recently, adaptive algorithms have also been presented, based on band-variable filters which are recursively updated as the signal is collected (Klepka and Uhl 2014, Quqa *et al*. 2021), or at given intervals (Quqa *et al*. 2020), to preserve efficiency and be suitable for implementation in battery-powered WSSNs. The S-transform (Stockwell 1996) has also received extensive interest due to its frequency-dependent resolution analysis, enabled by a Gaussian-windowed complex exponential, the dimensions of which scale as a function of frequency. This transform is at the base of the interpolation evolution method (Iacovino *et al*. 2018), which is an extension of the IM (Limongelli 2014) that demonstrated to be particularly effective for damage localization over most commonly used curvature-based techniques (Giordano and Limongelli 2020).

Herein, in order to enable real-time damage identification, instantaneous modal amplitudes are identified through a clustered filter bank (CFB)-based procedure (Quqa *et al*. 2020). The IM is thus applied using these values. The combination of CFB and IM, together with improvements specifically designed for decentralized applications, enable efficient and onboard damage localization. The issue related to the choice of the boundary conditions for each subset of sensors is tackled through two different approaches. The first approach is named Clump Interpolation Method (CIM) and assigns a not-a-knot condition at the ends of the interpolation interval; in the second approach, addressed to as Clamped Clump Interpolation Method (C^2IM), the boundary conditions are retrieved from the modal amplitudes identified in the reference (undamaged) configuration. The proposed method is applied to identify damage using the data collected by Vienna Consulting Engineers (VCE) and University of Tokyo during an experimental campaign conducted in 2008 on the S101 Bridge, in Austria (Siringoringo *et al*. 2013, VCE 2009).

The paper is structured as follows. Section 2 introduces the CFB-based procedure for modal identification. Section 3 describes the original IM for damage localization formulated in terms of modal shapes. Sections 4 and 5 are the core of the paper: Section 4 outlines the two novel decentralized methods for onboard SHM based on the CFB-based procedure and the IM, i.e., the CIM and the C^2IM, while Section 5 presents the results obtained by applying the two methods on the S101 Bridge. In particular, Section 5.1 presents the case study, Section 5.2 investigates the influence on the boundary conditions in the evaluation of the DSFs, Section 5.3 studies the effect on results of different sensor configurations, and Section 5.4 shows the results of a real-time SHM simulation. Concluding remarks are finally reported.

2. Clustered filter banks

Clustered filter banks were proposed in (Quqa *et al*. 2020) to perform signal processing operations for real-time modal identification of time-varying systems onboard decentralized WSSNs. The identification procedure consists of two steps. In the initialization step, a CFB is formed using a set of training signals collected at selected locations on the structure. This step is performed in a centralized fashion at the beginning of the procedure and may be repeated at user-defined time intervals to update the CFB if the structure changes due to damage or environmental variations. The second step is performed onboard each node and consists of a real-time analysis where the CFB is employed to extract decoupled modal contributions from the acquired structural responses. The modal contributions are exploited for the evaluation of instantaneous modal parameters through time-domain procedures, such as the Hilbert transform or nonlinear energy operator-based approaches. Interested readers may refer to (Quqa *et al*. 2020) for a complete description of the CFB-based method. In this section, a brief summary of the technique to build the CFB is reported, together with the outline of the procedure for using the filtered responses for damage identification.

In the first step, a set of training signals $\bar{x}_i[t]$, with $i = 1, \dots, r$, of length s is recorded at all the r sensor locations and transmitted to a central node. Here, each signal is decomposed through the stationary wavelet packet transform (SWPT) into k components (or sub-bands) $w_{i,k}[t]$, each with a narrow frequency band. The mentioned wavelet components can be calculated by applying equivalent wavelet filters to the collected signals, generated upon selecting a suitable wavelet function and a transform level (Quqa *et al.* 2020, Vetterli and Kovačević 1995). In this study, the impulse response of these equivalent filters are indicated as $b_k[h]$ and are calculated as $b_k[h] = (d_k * r_k)[h]$, where $*$ is the convolution operator, and $d_k[h]$, $r_k[h]$ are the impulse responses of equivalent decomposition and reconstruction SWPT filters, respectively. The $b_k[h]$ filters are, therefore, bandpass filters able to select narrow frequency bands (i.e., a sub-bands) of the collected signal. In the time domain, at the i-th sensor location, the k-th sub-band thus provides a contribution $w_{i,k}[t]$ to the response at time t. The normalized contribution of the k-th sub-band, that will be addressed herein as sub-band shape (SBS), can be defined as

$$\varphi_{i,k} = \frac{1}{s}\sum_{t=1}^{s}\frac{w_{i,k}[t]}{w_{ref,k}[t]} \tag{1}$$

where $w_{ref,k}[t]$ is the k-th sub-band contribution at a reference sensor location. The sub-band contribution can either coincide or not with modal responses. The CFB-based identification procedure used in this study is based on the idea that the narrow-band contributions $w_{i,k}[t]$ generated from a set of structural responses will form SBSs which are similar to each other if they refer to the same modal response. Moreover, due to the orthogonality property of vibration modes, the SBSs of two different modal responses will likely be orthogonal. In order to separate the modal responses within all the sub-band contributions, the similarity between the adjacent SBSs $\boldsymbol{\varphi}_k$ and $\boldsymbol{\varphi}_{k+1}$, formed of the elements of Eq. (1), is tested using the modal assurance criterion (MAC): High MAC values denote similar SBSs, possibly associated with a unique vibration mode. Here, $\boldsymbol{\varphi}_k$ indicates the vector containing the SBS related to the k-th sub-band calculated for all the instrumented locations. This can be interpreted as an instantaneous operating deflection shape of the structure.

Once one SBS is determined for each sub-band, sub-bands with similar SBSs (i.e., SBSs having MAC value that exceeds a user-defined threshold) are thus partitioned into clusters. The $b_k[h]$ filters employed to obtain the wavelet components (and the SBSs) of each cluster are then summed up to obtain a new 'clustered' filter $\bar{b}_j[h]$ with larger cutoff frequencies corresponding to the frequency range of a modal response. The sum of the $b_k[h]$ filters is possible thanks to the perfect reconstruction property (Vetterli and Kovačević 1995). Filters $\bar{b}_j[h]$ corresponding to negligible contributions (i.e., low-amplitude contributions) to the response can be discarded using energy-based selection procedures.

The first phase of the identification procedure ends with the computation of the clustered filters $\bar{b}_j[h]$ that form the CFB. In the second phase, the CFB is used for extracting decoupled modal responses from the recorded response by convolution

$$y_{i,j}[t] = \sum_{h=0}^{N-1} x_i[t-h]\,\bar{b}_j[h] \tag{2}$$

where $x_i[t]$ is the signal acquired at the i-th location and N is the length of $\bar{b}_j[h]$. CFBs are generally able to accommodate modest variations in structural responses due to non-stationarities and operational effects. However, such filters should be updated in the aftermath of stronger modifications due to damage or considerable environmental variations. Although a fully adaptive procedure to determine the CFB offline is proposed in (Quqa *et al.* 2021), the original formulation reported in this section is more suitable for onboard processing, due to its limited computational complexity.

3. Interpolation method

The idea behind the IM (Limongelli 2014) is that by using a smooth (e.g., a cubic spline) function to interpolate deflection shapes, the interpolation error is higher at sections with discontinuities of stiffness thereby a localized loss of stiffness causes an increase of the interpolation error. The DSF is therefore defined as a variation between a baseline and an inspection configuration of the interpolation error. In both configurations, the interpolation error is evaluated at a given location i as the difference between the value of the deflection amplitudes retrieved from the signal measured at i and the value of the same amplitude obtained through interpolation of the amplitudes extracted from all the other measured responses. The IM has been originally formulated in terms of operating deflection shapes of the structures retrieved by frequencies response functions computed at each instrumented location (Limongelli 2010). Herein, the IM is formulated using modal shapes (Giordano and Limongelli 2020) which are obtained through the clustered filter bank CFB-based procedure described in the previous section. The interpolation error at location i calculated considering p vibration modes is given by

$$E_i = \sqrt{\sum_{j=1}^{p}\left|\phi_{j,i} - \hat{\phi}_{j,i}\right|^2} \tag{3}$$

where $\phi_{j,i}$ indicates the i-th component of the j-th modal shape and $\hat{\phi}_{j,i}$ is the value at the same location obtained by interpolation. In particular, the value $\hat{\phi}_{j,i}$ is obtained as follows: (1) removal of the i-th component of the j-th modal shape; (2) estimation of the value of the j-th modal shape at the i-th location by interpolating the remaining values of the mode shape with a cubic spline function. The procedure is repeated for all the components of the mode shapes, excluding the end nodes. The damage indicator is defined as the positive difference between the values of the interpolation error in a possibly damaged (D) and on the reference (U) states

$$\Delta E_i = E_{i,D} - E_{i,U} \tag{4}$$

The coefficients of the cubic spline function are determined by imposing the continuity of the function, and its first and second derivatives at all the knots (i.e., the interpolation points). Two additional conditions must be imposed at the boundaries of the interpolation domain to uniquely determine the coefficients of the spline function. The conditions should satisfy the physical constraints at the boundary: For example, in the case of a simply supported beam, a zero curvature (null bending moment) can be imposed giving rise to a so-called "natural spline"; in the case of a clamped constraint, a zero rotation condition must be imposed. A further option is to require the continuity of the third derivative (related to shear) at the second and the second-last knots. This condition is generally referred to as the "not-a-knot" condition and is equivalent to use a single cubic polynomial to interpolate the data at the first and last three knots. The different boundary conditions do not sensibly affect the value of the interpolation error at locations far from the boundary.

The IM is a method for damage localization whose application is envisaged to identify localized irregularities in the mode shapes of the structure. The capability of the IM to detect multiple damaged locations has been demonstrated in several papers (Domaneschi *et al*. 2013a, b, Limongelli 2014) considering different structural types. In the case of a diffuse damage, the damage location is not circumscribed. Thereby, methods for damage detection (i.e., those based on natural frequencies as damage feature), provide the required information at a lower effort since they generally require a much smaller number of sensors.

4. Decentralized approach for onboard structural health monitoring

The traditional formulation of the IM for damage identification relies on the data collected by the complete set of sensors deployed on the structure. In this paper, spatial subdomains are investigated individually, involving the evaluation of local DSFs based on the recordings collected by small groups of neighboring sensing devices. Therefore, this procedure involves approximations in the interpolation of the modal shapes, mainly due to the boundary conditions at the edges of the subdomains. In this section, two decentralized variants of the IM, the CIM and the C^{2}IM are described. The two variants differ in terms of boundary conditions imposed at the edges of each subset of sensors. Using the IM as a DSF requires a careful choice of the boundary conditions in order to reduce their influence on the outcome of damage localization performed on spatially limited portions (spatial subdomains) of the structure corresponding to the locations of the node groups. The procedure proposed herein is organized in two steps, the first for the initialization of the procedure and the second for real-time damage localization.

4.1 Step 1: Initialization

The first step involves the formation of a CFB and the construction of the baseline parameters employed in the next step of the procedure for damage identification. These parameters consist of an estimation of the "baseline" modal shapes, their rotations at the knots (i.e., the instrumented locations), and the values of the interpolation error in the baseline configuration.

The formation of the CFB consists of the process described in Section 2. In particular, in the first step, all the sensing devices collect a signal interval that is transmitted to a central node. Here, the structural responses are filtered through the equivalent decomposition SWPT filters generating 2^n narrow-band components (with n denoting the level of the transform). The SBSs are then evaluated for each sub-band k as shown in Eq. (1) and partitioned through the MAC-based criterion into different clusters, each related to a different vibration mode. The j-th clustered filter is thus calculated by summing the impulse responses $b_k[h]$ of the filters that generated SBSs contained in the j-th cluster. The $\bar{b}_j[h]$ filters thus obtained form the CFB. Moreover, the SBSs $\varphi_{i,k}$ contained in the j-th cluster are averaged to compute the j-th baseline modal shape. The i-th component of the j-th modal shape in the baseline configuration is thus given by

$$\bar{\phi}_{i,j} = \frac{1}{m}\sum_{k=1}^{m} \varphi_{i,k} \tag{5}$$

where m is the number of SBSs in the j-th cluster. The baseline modal shapes computed through Eq. (5) are then employed to calculate the values of the first derivatives (rotations) at the knots $\bar{\phi}'_{i,j}$. This can be done by using the forward, backward, or central difference method. In the second step of the procedure, if the C^{2}IM is adopted, these rotations will be used to impose a clamped condition at the boundary of each subset of sensors, both in the baseline and inspection configurations. This is done neglecting the difference in the boundary rotations that may arise between the two configurations due to damage or noise-related uncertainties. On the other hand, in the CIM approach, the boundary conditions are imposed through not-a-knot conditions. Therefore, using the CIM, the values of the $\bar{\phi}'_{i,j}$ are not evaluated in this first step. The baseline values of the interpolation error at all the knots are also calculated in this phase using the procedure described in Section 3.

Step 1 is generally characterized by a higher computational burden over step 2: See (Quqa *et al*. 2020) for a detailed quantification. However, it should be performed only at the beginning of the procedure or at the occurrence of severe damage or strong environmental variations if the filter banks evaluated for the baseline condition become no more suitable for the inspections due to substantial changes in the modal parameters. It should be noted that, limited to this phase, computations may be performed in cloud computing platforms or onboard a central node with a larger computational footprint and wired power supply.

4.2 Step 2: Real-time damage identification

Once the initialization step is completed, the CFB is transmitted to each node of the sensor network. Also, the values of the baseline rotations at the knots (needed by the

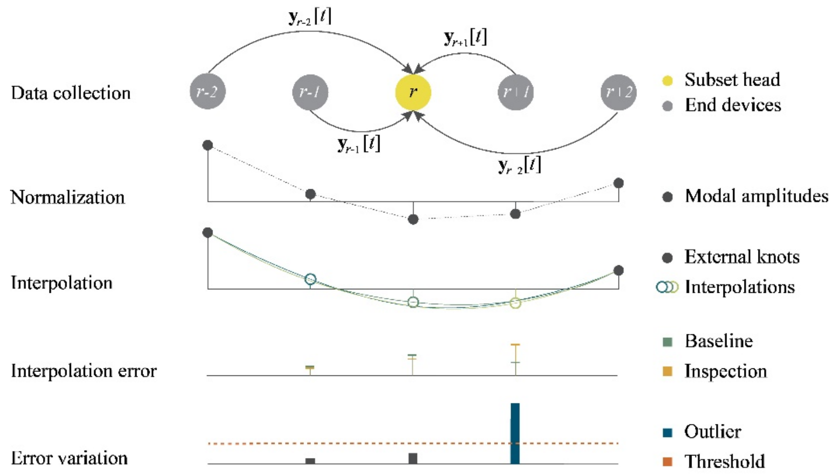

Fig. 1 Schematic of the procedure proposed referred to a single sensor subset

C²IM to impose the clamped conditions) and the baseline interpolation error are transmitted to selected "subset heads", where the computation of DSF takes place (Fig. 1). Subset heads should be located in a central position within each subset of nodes to allow wireless transmission from all the end devices (i.e., the sensors in the subset except the head).

The sensor network is designed with a hierarchical tree structure, that is, each node has a specific function: At each time t, all the nodes collect new samples of the structural response and extract (onboard) the p modal responses $\mathbf{y}_i[t] = \left(y_{i,1}[t], \dots, y_{i,p}[t]\right)$ through the CFB, using Eq. (2); then, each end device transmits the relevant modal responses $\mathbf{y}_i[t]$ to the head of the subset(s) it belongs to. Here, for each time instant, the components of each j-th mode ($j = 1, \dots p$) are normalized to the component of the same mode calculated at the r-th location ($y_{r,j}[t]$), related to the subset head, as follows

$$\phi_{i,j}[t] = \frac{y_{i,j}[t]}{y_{r,j}[t]} \tag{6}$$

The interpolation error and its variation with respect to the baseline values are thus computed onboard each subset head employing the portions of normalized modal shapes calculated using the data collected in the related sensor groups. One of the two approaches (CIM or C²IM) for selecting the boundary conditions at the edges of the spatial subdomains is employed in this phase to calculate the interpolations. If the value of the interpolation error is identified as an outlier with respect to the history of previous values, an alert is given by the system. In order to limit the occurrence of false alarms due to the presence of time-localized outliers, a median filter may be implemented onboard the group head, keeping in memory a defined number of interpolation error sets.

In general, the interpolating cubic spline is defined by a set of different polynomials, one for each interval between consecutive knots. When the number of nodes in a single subset does not exceed 5 and the CIM approach is used to impose the boundary conditions, the interpolating function degenerates into a polynomial (cubic, quadratic, or linear if the subsets are formed by 5, 4, or 3 nodes, respectively) which is unique across the entire group of instrumented locations. In this condition, the normalized percent variation of the interpolation error, computed as

$$\Delta^{\%} E_i = 100 \frac{E_{i,D} - E_{i,U}}{E_{i,U}}, \tag{7}$$

is constant across all the nodes in one group (the proof is reported in Appendix). Thereby, this value can be computed once, at the group head, where all the data are transmitted by the other nodes. On the other hand, when large sensor groups or C²IM are employed, the variation described in Eq. (7) is different for each instrumented location and should be computed separately.

It is worthy to note that, depending on the application, the proposed procedure can be performed in real time, evaluating the DSF as new data is collected, and continuously. However, in civil applications, event-triggered approaches or periodic inspections may be scheduled to preserve the battery of sensing devices, turning them in the sleeping mode for most of the time. In the Applications section of this paper, both the approaches are tested.

5. Applications

In this section, practical applications of the methods proposed are shown, using the ambient vibration data collected by the Vienna Consulting Engineers (VCE) during an experimental campaign conducted in 2008 on the S101 Bridge, in Vienna, Austria (Siringoringo *et al*. 2013, VCE 2009).

5.1 Description of the case study

The case study, represented in Fig. 2, consists of a post-tensioned three-span concrete bridge, built in the 1960s and demolished in 2008. The slab was continuous and divided by two pairs of piers in a central and two side spans of 32 and 12 m, respectively. The cross-section consisted of two beams with variable height along the longitudinal direction,

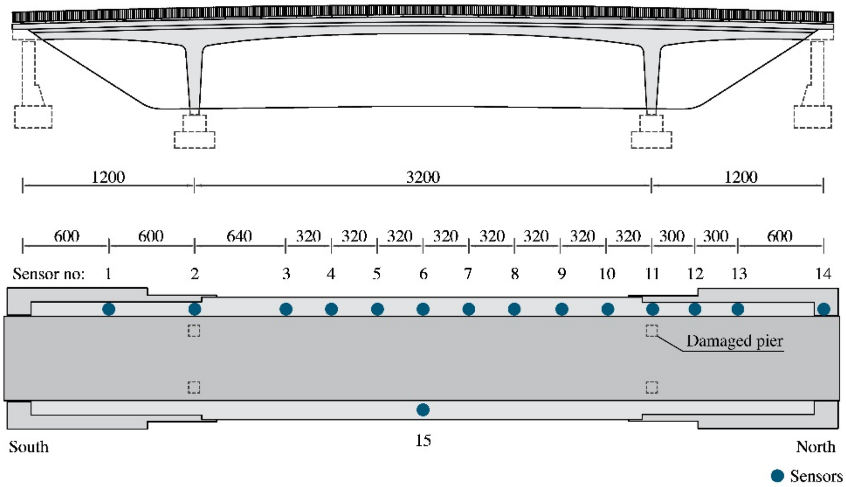

Fig. 2 Case study and sensor deployment, adapted from (VCE 2009), dimensions in centimeters

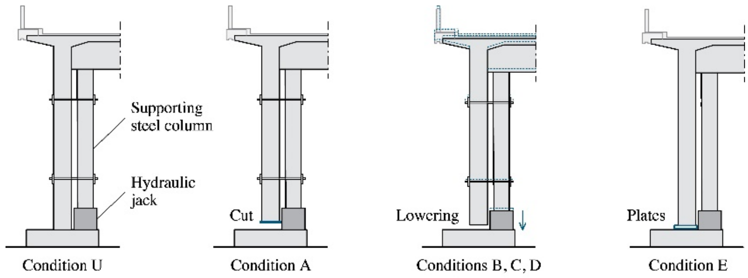

Fig. 3 Schematic of progressively induced damage scenarios

equal to 0.9 m in the middle of the central span, up to 1.7 m at the piers, with a constant total width of 7.2 m. Vibration data were collected using a dense BRIMOS (Döhler *et al.* 2014, Wenzel and Pichler 2005) network, deployed as reported in Fig. 2, consisting of 15 three-directional FBA-23 force balance accelerometers from Kinemetrics, with a sensitivity of 2.5 V/g under a full-scale range of 1 g, and a resolution of 10^{-6} g. Raw data were logged using a 16-bit analog-to-digital converter (ADC). Data were originally acquired with a sampling frequency of 500 Hz.

In this application, only accelerations collected by sensors 1-14 in the vertical direction, downsampled at 100 Hz, are used. Before the demolition, a three-day experimental campaign was carried out, inducing progressive damage consisting of north-western pier settlements and loss of post-tension forces. In this study, only the pier settlement conditions are considered (see Fig. 3).

First, the pier was unloaded using a hydraulic jack. Then, it was cut at the base (condition A) and a slice of 10 cm was removed. The jack was then lowered in three progressive steps, each by 1 cm (conditions B, C, and D). At the end of the third step, in condition D, the final measured settlement was 2.7 cm, and the column was completely suspended. In condition E, some compensating plates were inserted at the bottom of the pier. In this study, a set of 14 acceleration time histories (i.e., one per sensor location) of 330 s were analyzed for each damage condition. The training signal for the construction of the first CBF, of the boundary conditions, and of the baseline interpolation error was selected considering the first 165s of the responses relevant to condition U. An update of CFB was performed to filter the responses referred to each further damage condition. In order to simulate the operations that would be performed onboard individual sensors for the extraction of decoupled modal responses, each signal was individually processed through the CBF.

The CBFs were obtained using the SWPT, through the 22-nd order Fejér-Korovkin wavelet (fk22), up to a decomposition level 7. Three vertical bending modes, with frequencies equal to respectively 3.98 Hz, 9.61 Hz, and 12.47 Hz in the undamaged condition, and one torsional mode, with frequency 6.18 Hz in the undamaged condition, were extracted. More details on the CFB and the decomposition of structural responses can be found in (Quqa *et al.* 2020) where the case study is analyzed in detail.

5.2 Influence of the boundary conditions in damage identification

In this section, the results of the decentralized damage identification procedure obtained for the S101 Bridge are reported together with an investigation of the effects of the boundary conditions on the results. Only the first three modal shapes are used for the evaluation of the damage indicator according to Eqs. (3) and (7), due to the high level of uncertainties related to the fourth mode. In this section, modal amplitudes are evaluated as the average values of the instantaneous estimates provided by Eq. (6) over a 330 s

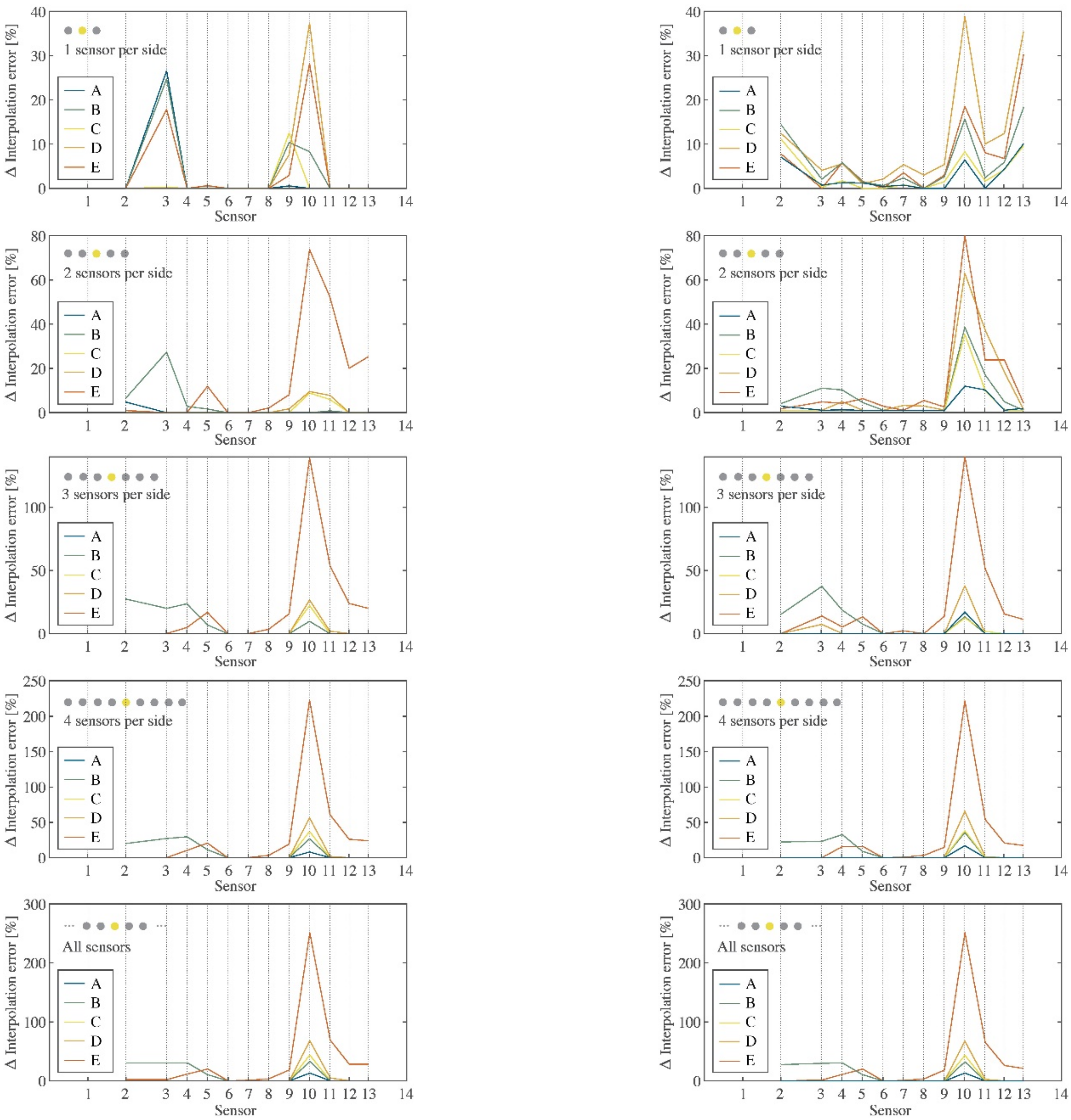

(a) Clump Interpolation Method

(b) Clamped-Clump Interpolation Method

Fig. 4 Percent difference of the interpolation error at subset heads

window for each damage condition.

Fig. 4 displays the values of the damage index computed using both the CIM and the C^{2}IM and considering a different number of sensors in the subset of sensors (specifically one, two, three, four, and all the sensors at each side of the subset head). For the nodes close to the ends of the deck, the available sensors are considered. A scheme of the sensor layout, with the subset head indicated in yellow, is reported in the upper-left part of each figure. The figure reports, for each location, the value of the damage index computed assuming that location as subset head and the sensor layout indicated in the scheme. The last configuration, where all sensors are employed, provides the same results of the original centralized IM algorithm. The high values of the damage index at location 10 are explained by the fact that cutting and lowering the pier at location 11 is likely to have caused damage also at the neighboring locations. Furthermore, the interpolation technique tends to "spread" the effect of damage at neighboring locations (Limongelli 2010). However, the IM is proposed as a global damage localization method able to provide a gross identification of the damaged portion of the structure that can guide infrastructure operators in the selection of further investigations. In this perspective, the level of approximation provided by the method is considered appropriate. In general, the DSF increases with the severity of the damage (configurations A to E). At the increase of the number of sensors per side, the values of the DSF approach to those of the original algorithm: Both for the CIM and C^{2}IM, with 7 sensors (3 sensors for each side of the subset head), the values of the DSF are almost coincident to the ones of the original IM.

In this study, the damage index is defined as the ratio of the variation of the interpolation error between the inspection and baseline configurations and its value in the undamaged configuration (see Eq. (7)). Due to the presence of the southern pier, sensors 2 and 3 are close to a node of the modal shapes, thereby the denominator of the damage

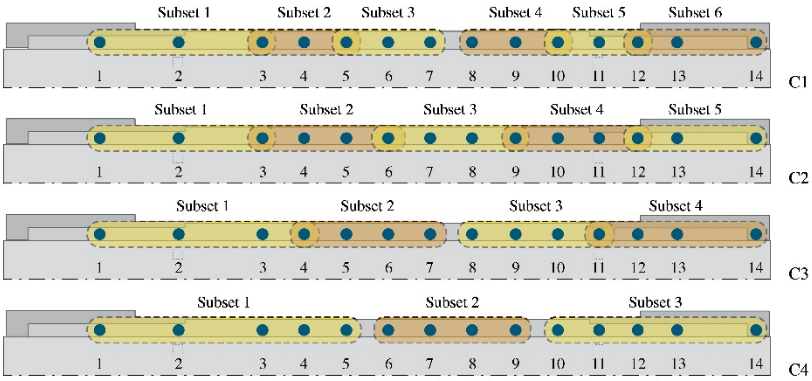

Fig. 5 Sensor configurations

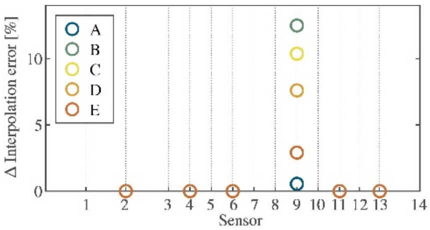

(a) Configuration C1 – CIM

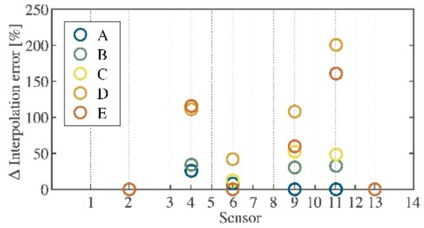

(b) Configuration C1 – C^{2}IM

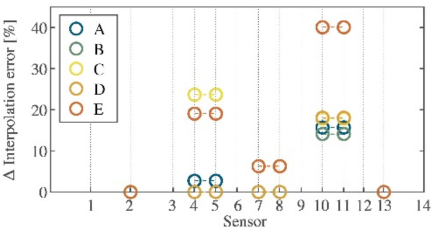

(c) Configuration C2 – CIM

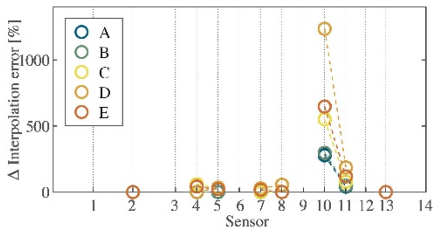

(d) Configuration C2 – C^{2}IM

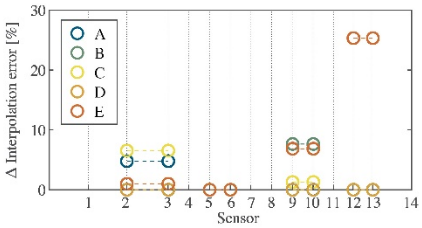

(e) Configuration C3 – CIM

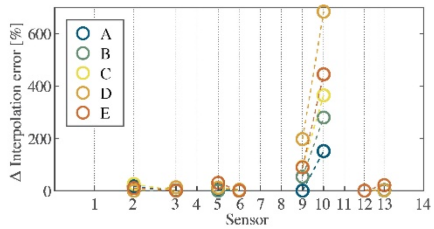

(f) Configuration C3 – C^{2}IM

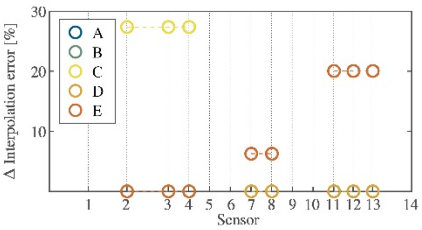

(g) Configuration C4 – CIM

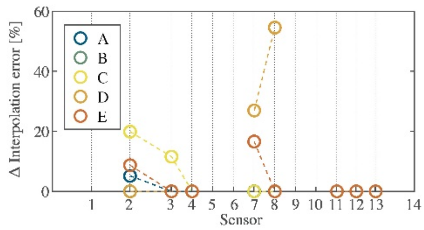

(h) Configuration C4 – C^{2}IM

Fig. 6 Percent difference of the interpolation error evaluated through the CIM and C^{2}IM

index at these two locations is generally small. A slight variation of the interpolation error may thus involve high values of the damage index, which may generate false positives. This is emphasized if few sensors are included in the cluster due to the increasing relevance of the effects of the boundary conditions. However, the analyses of the time history of the damage index highlight that these high values occur at a limited number of instants and can be considered as false alarms related to computational errors and noise.

5.3 Periodic damage identification

In this section, the performance of CIM and C^{2}IM is investigated using four different sensor configurations, as illustrated in Fig. 5. Periodic inspections are simulated and the modal shapes were computed considering the average values over signal windows of 330 s for each damage condition.

All sensor configurations have been selected with a symmetric layout, considering the 14 acquisition channels with some overlap. In particular, configuration C1 consists of six subsets formed by three sensors each, with four shared nodes (3, 5, 10, and 12) that transmit modal responses to both subsets they belong to. Similarly, configurations C2, C3, and C4 are formed by 5, 4, and 3 subsets, respectively, with an increasing number of sensors for each subset. It should be noted that shared nodes should be avoided in large subsets to limit transmission overloads.

In Fig. 6, the values of the damage index obtained at each sensor through the CIM and C^{2}IM, respectively, are reported. Differently from the results shown in the previous section, here the DSF is evaluated at each sensor location, except the external knots which cannot be interpolated. As mentioned in Section 4.2, the values of the damage index computed using the CIM are constant within each subset whereas those provided by C^{2}IM can change from one node to the other of the same subset.

The comparison of results shows that considerable improvement can be obtained including the clamped conditions in the interpolation process, that is, using the C^{2}IM, although these conditions are evaluated only at the beginning of the procedure, in the baseline condition (scenario U), neglecting the possible variation of the modal shape rotations due to the damage. Using C^{2}IM, configurations C2 and C3, provide a clear indication of damage close to sensor 11 for each damage condition. The CIM generally provides higher values of the DSF close to location 11 but results are less accurate with respect to the C^{2}IM. Concerning configuration C4, less accurate localization of damage is obtained using both methods. This result may be due to the fact that the location of the damage is in the spatial subdomain covered by an external subset of sensors, that is, close to the end of the deck. Thereby, in this case, the values of the damage indices are evaluated applying a not-a-knot boundary condition on the right side of the subset. Considering configuration C1, the CIM seems to perform better than C^{2}IM. However, observing Fig. 4, different outliers can be noticed, leading to a misleading damage localization.

Considering the subset of locations where damage indices are evaluated in configuration C1, the outliers in the first part of the deck are not visible. Nevertheless, using C^{2}IM in configuration C1, higher values in the DSF are generally registered in the second half of the deck. It should also be noted that the values of the damage index computed with the C^{2}IM approach are much higher with respect to those obtained with the CIM because the values of the interpolation error relevant to the baseline condition are very low in the first case.

5.4 Real-time damage identification

In this section, the analyses are conducted simulating real-time online damage identification. In particular, 14 acceleration time histories (i.e., one for each sensor location) of 33 minutes were generated by merging the signals, of length 330-seconds, relevant to conditions U, A, B, C, D, and E. In Figs. 7-8, the results obtained using CIM and C^{2}IM, respectively, are reported.

In order to simulate the real-time operations performed

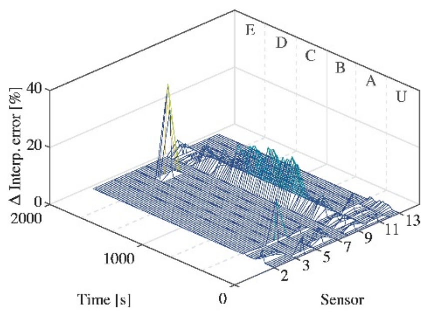

(a) Configuration C1

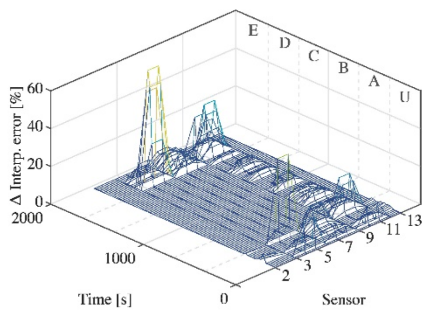

(b) Configuration C2

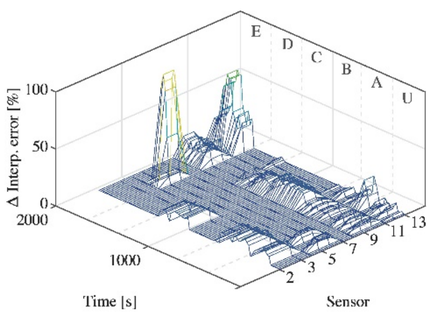

(c) Configuration C3

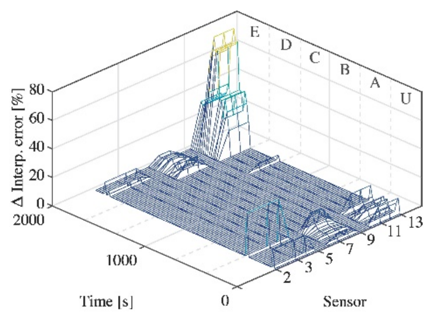

(d) Configuration C4

Fig. 7 Simulation of a real-time damage identification procedure through the CIM

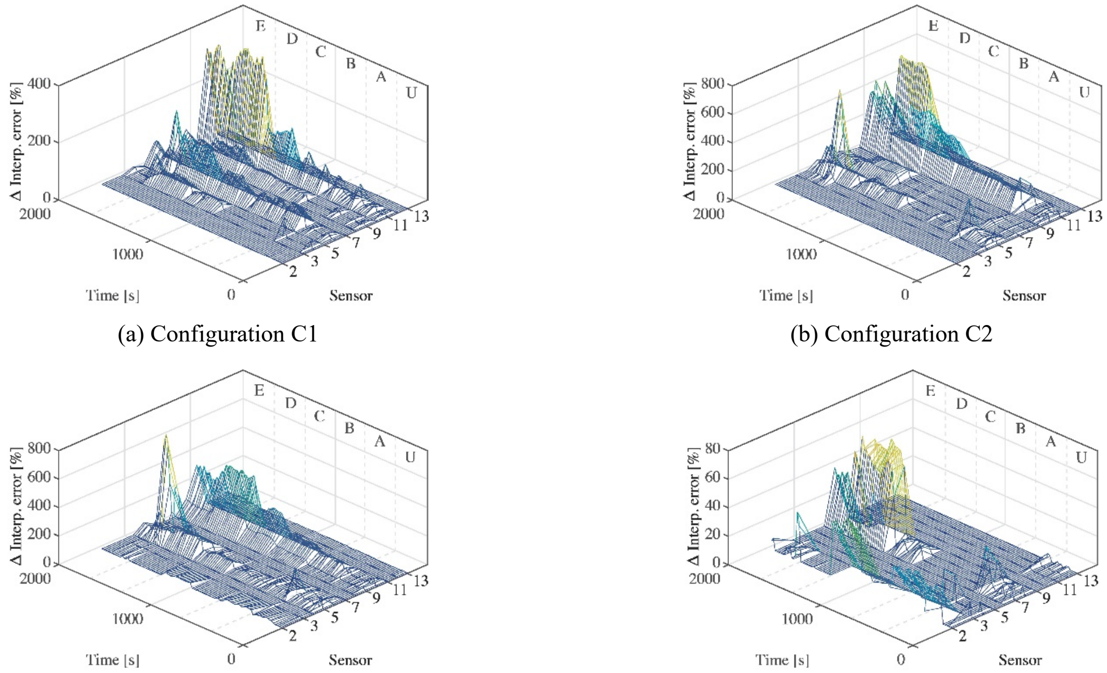

(a) Configuration C1 (b) Configuration C2

(c) Configuration C3 (d) Configuration C4

Fig. 8 Simulation of a real-time damage identification procedure through the C^{2}IM

onboard each node, the procedure outlined in Section 4 to extract the modal contributions was applied to each signal individually. At each time, the component of the modal shape is assumed as the median value computed on the previous 1000 samples (i.e., 10 s). The first three instantaneous modal shapes were computed according to Eq. (6) and used to evaluate the damage indices. The use of the CIM provides a single value of the damage index for each subset which enables to reduce the computation burden when online processing is performed. However, the identification of damage is less accurate with respect to that performed by the C^{2}IM: Several missing alarms occur, especially in configurations C3 and C4. Nevertheless, the persistence of positive outcomes enables us to distinguish between persistent damage and localized outliers which may be due to noise and non-stationarities in the structural response. Moreover, considerable improvements are obtained using the C^{2}IM as shown by the results obtained for configurations C1, C2, and C3, providing accurate localization for all damage conditions, with limited localized outliers, especially in condition E. Configuration C4 does not enable localization up to damage scenario C and for scenarios D and E indicates damage near to sensor 9.

6. Conclusions

In this paper, two decentralized variants of the interpolation method (IM) for damage identification have been proposed to enable the use of smart wireless sensor networks through the formation of subsets of sensors.

A preliminary study was conducted to prove the suitability of the IM for decentralized applications, showing how the inclusion of clamped boundary conditions retrieved from the baseline structure, which are adopted in the Clamped-Clump Interpolation Method (C^{2}IM), critically improves results with respect to the simpler Clump Interpolation Method (CIM). However, the CIM has resulted particularly suitable for online implementations due to its lower computational burden enabled by the possibility to compute a single value of the damage index for each subset rather than for each sensor. Due to the same property, damage can only be localized with the resolution corresponding to the sensor subset. Moreover, in a real-time approach, the evolution in time of the damage index may enable the user to discern actual damage from localized outliers generated by noise and short-term operational conditions.

The investigation of the sensitivity of results to the sensor configurations pointed out the need for further investigations to identify the optimal design for damage localization purposes.

Acknowledgments

The authors would like to thank the Vienna Consulting Engineers (VCE) company for providing the data recorded during the experimental campaign carried out on the S101 Bridge.

References

Avci, O., Abdeljaber, O., Kiranyaz, S., Hussein, M. and Inman, D.J. (2018), “Wireless and real-time structural damage detection: A novel decentralized method for wireless sensor networks”, *J. Sound Vib.*, **424**, 158-172. https://doi.org/10.1016/j.jsv.2018.03.008

Brincker, R. and Ventura, C.E. (2015), *Introduction to Operational*

Modal Analysis, John Wiley & Sons, Ltd.
Daubechies, I. (1992), Ten Lectures on Wavelets.
Döhler, M., Hille, F., Mevel, L. and Rücker, W. (2014), "Structural health monitoring with statistical methods during progressive damage test of S101 Bridge", *Eng. Struct.*, **69**, 183-193. https://doi.org/10.1016/j.engstruct.2014.03.010
Domaneschi, M., Limongelli, M.P. and Martinelli, L. (2013a), "Multi-site damage localization in a suspension bridge via aftershock monitoring", *Int. J. Earthq. Eng.*, **30**(3), 56-72.
Domaneschi, M., Limongelli, M.P. and Martinelli, L. (2013b), "Vibration based damage localization using MEMS on a suspension bridge model", *Smart Struct. Syst., Int. J.*, **12**(6), 679-694. http://dx.doi.org/10.12989/sss.2013.12.6.679
Gabor, D. (1946), "Theory of communication. Part 1: The analysis of information", *J. Inst. Elect. Engr. - Part III: Radio and Commu. Eng.*, **93**(26), 429-441. https://doi.org/10.1049/ji-3-2.1946.0074
Gao, Y., Spencer, B.F. and Ruiz-Sandoval, M. (2006), "Distributed computing strategy for structural health monitoring", *Struct. Control Health Monitor.*, **13**(1), 488-507. https://doi.org/10.1002/stc.117
Giordano, P.F. and Limongelli, M.P. (2020), "Response-based time-invariant methods for damage localization on a concrete bridge", *Struct. Concrete*, **21**(4), 1254-1271. https://doi.org/10.1002/suco.202000013
Iacovino, C., Ditommaso, R., Ponzo, F.C. and Limongelli, M.P. (2018), "The Interpolation Evolution Method for damage localization in structures under seismic excitation", *Earthq. Eng. Struct. Dyn.*, **47**(10), 2117-2136. https://doi.org/10.1002/eqe.3062
Jang, S., Jo, H., Cho, S., Mechitov, K., Rice, J.A., Sim, S.H., Jung, H.J., Yun, C.B., Spencer, B.F. and Agha, G. (2010), "Structural health monitoring of a cable-stayed bridge using smart sensor technology: Deployment and evaluation", *Smart Struct. Syst., Int. J.*, **6**(5-6), 439-459. https://doi.org/10.12989/sss.2010.6.5_6.439
Kaya, Y. and Safak, E. (2015), "Real-time analysis and interpretation of continuous data from structural health monitoring (SHM) systems", *Bull. Earthq. Eng.*, **13**(3), 917-934. https://doi.org/10.1007/s10518-014-9642-9
Kijewski, T. and Kareem, A. (2003), "Wavelet transforms for system identification in civil engineering", *Comput.-Aided Civil Infrastruct. Eng.*, **18**(5), 339-355. https://doi.org/10.1111/1467-8667.t01-1-00312
Klepka, A. and Uhl, T. (2014), "Identification of modal parameters of non-stationary systems with the use of wavelet based adaptive filtering", *Mech. Syst. Signal Process.*, **47**(1-2), 21-34. https://doi.org/10.1016/j.ymssp.2013.09.001
Li, J., Su, M. and Fan, L. (2003), "Natural frequency of railway girder bridges under vehicle loads", *J. Bridge Eng.*, **8**(4), 199-203. https://doi.org/10.1061/(ASCE)1084-0702(2003)8:4(199)
Limongelli, M.P. (2010), "Frequency response function interpolation for damage detection under changing environment", *Mech. Syst. Signal Process.*, **24**(8), 2898-2913. https://doi.org/10.1016/j.ymssp.2010.03.004
Limongelli, M.P. (2014), "Seismic health monitoring of an instrumented multistory building using the interpolation method", *Earthq. Eng. Struct. Dyn.*, **43**(11), 1581-1602. https://doi.org/10.1002/eqe.2411
Long, J. and Büyüköztürk, O. (2017), "Decentralised one-class kernel classification-based damage detection and localisation", *Struct. Control Health Monitor.*, **24**(6), 1-22. https://doi.org/10.1002/stc.1930
Nagarajaiah, S. and Basu, B. (2009), "Output only modal identification and structural damage detection using time frequency & wavelet techniques", *Earthq. Eng. Eng. Vib.*, **8**(4), 583-605. https://doi.org/10.1007/s11803-009-9120-6
Nagayama, T., Spencer, B.F. and Rice, J.A. (2009), "Autonomous decentralized structural health monitoring using smart sensors", *Struct. Control Health Monitor.*, **16**(7-8), 842-859. https://doi.org/10.1002/stc.352
Nguyen, K.V. (2013), "Comparison studies of open and breathing crack detections of a beam-like bridge subjected to a moving vehicle", *Eng. Struct.*, **51**, 306-314. https://doi.org/10.1016/j.engstruct.2013.01.018
Pakrashi, V., O'Connor, A. and Basu, B. (2010), "Effect of tuned mass damper on the interaction of a quarter car model with a damaged bridge", *Struct. Infrastruct. Eng.*, **6**(4), 409-421. https://doi.org/10.1080/15732470701816850
Quqa, S., Landi, L. and Diotallevi, P.P. (2020), "Instantaneous modal identification under varying structural characteristics: A decentralized algorithm", *Mech. Syst. Signal Process.*, **142**, 106750. https://doi.org/10.1016/j.ymssp.2020.106750
Quqa, S., Landi, L. and Diotallevi, P.P. (2021), "Modal assurance distribution of multivariate signals for modal identification of time-varying dynamic systems", *Mech. Syst. Signal Process.*, **148**, 107136. https://doi.org/10.1016/j.ymssp.2020.107136
Rice, J.A., Mechitov, K., Sim, S.H., Nagayama, T., Jang, S., Kim, R., Spencer, B.F., Agha, G. and Fujino, Y. (2010), "Flexible smart sensor framework for autonomous structural health monitoring", *Smart Struct. Syst., Int. J.*, **6**(5-6), 423-438. https://doi.org/10.12989/sss.2010.6.5_6.423
Siringoringo, D.M., Fujino, Y. and Nagayama, T. (2013), "Dynamic characteristics of an overpass bridge in a full-scale destructive test", *J. Eng. Mech.*, **139**(6), 691-701. https://doi.org/10.1061/%28ASCE%29EM.1943-7889.0000280
Spiridonakos, M.D. and Fassois, S.D. (2009), "Parametric identification of a time-varying structure based on vector vibration response measurements", *Mech. Syst. Signal Process.*, **23**(6), 2029-2048. https://doi.org/10.1016/j.ymssp.2008.11.004
Stockwell, R.G. (1996), "Localization of the complex spectrum: the s transform", *IEEE Transact. Signal Process.*, **44**(4), 993. https://doi.org/10.1109/78.492555
VCE, Vienna Consulting Engineers (2009), Progressive damage test S101 - Flyover reibersdorf, Report nr. 08/2308.
Vetterli, M. and Kovačević, J. (1995), *Wavelets and Subband Coding*, Prentice Hall Ptr, Englewood Cliffs, NJ, USA.
Wenzel, H. and Pichler, D. (2005), Ambient Vibration Monitoring, John Wiley and Sons Ltd.

Appendix: Proof of Eq. (7)

In this Appendix, the proof of Eq. (7) reported in Section 4.2 is given for the case of a cubic polynomial, i.e., for subsets of 5 sensors. This proof is however general and also applicable for smaller subsets.

Considering the equation of a cubic polynomial in the form

$$f(x) = ax^3 + bx^2 + cx + d \tag{A1}$$

the i-th element of the j-th modal shape in the undamaged (U) condition, can be written as

$$\phi_{j,i}^U = a_{j,i}^U {x_i}^3 + b_{j,i}^U {x_i}^2 + c_{j,i}^U x_i + d_{j,i}^U \tag{A2}$$

where x_i is the location of the i-th sensor, and the coefficients may be organized in a vector

$$\boldsymbol{\theta}_{j,i}^U = \left[a_{j,i}^U \; b_{j,i}^U \; c_{j,i}^U \; d_{j,i}^U\right]^T \tag{A3}$$

Considering for each location a vector

$$\mathbf{x}_i = [{x_i}^3 \; {x_i}^2 \; x_i \; 1]^T \tag{A4}$$

let the matrix $\mathbf{X}_i$ be formed by all vectors (A4) except the i-th

$$\mathbf{X}_i = [\mathbf{x}_1^T \ldots \mathbf{x}_{i-1}^T \; \mathbf{x}_{i+1}^T \ldots \mathbf{x}_5^T]^T \tag{A5}$$

The inverse of this matrix, due to its particular structure, can be written as

$$\mathbf{X}_i^{-1} = \begin{bmatrix} \frac{1}{(\xi_1-\xi_2)(\xi_1-\xi_3)(\xi_1-\xi_4)} & -\frac{1}{(\xi_1-\xi_2)(\xi_2-\xi_3)(\xi_2-\xi_4)} & \frac{1}{(\xi_1-\xi_3)(\xi_2-\xi_3)(\xi_3-\xi_4)} & -\frac{1}{(\xi_1-\xi_4)(\xi_2-\xi_4)(\xi_3-\xi_4)} \\ -\frac{\xi_2+\xi_3+\xi_4}{(\xi_1-\xi_2)(\xi_1-\xi_3)(\xi_1-\xi_4)} & \frac{\xi_1+\xi_3+\xi_4}{(\xi_1-\xi_2)(\xi_2-\xi_3)(\xi_2-\xi_4)} & -\frac{\xi_1+\xi_2+\xi_4}{(\xi_1-\xi_3)(\xi_2-\xi_3)(\xi_3-\xi_4)} & \frac{\xi_1+\xi_2+\xi_3}{(\xi_1-\xi_4)(\xi_2-\xi_4)(\xi_3-\xi_4)} \\ \frac{\xi_3\xi_4+\xi_2(\xi_3+\xi_4)}{(\xi_1-\xi_2)(\xi_1-\xi_3)(\xi_1-\xi_4)} & -\frac{\xi_3\xi_4+\xi_1(\xi_3+\xi_4)}{(\xi_1-\xi_2)(\xi_2-\xi_3)(\xi_2-\xi_4)} & \frac{\xi_2\xi_4+\xi_1(\xi_2+\xi_4)}{(\xi_1-\xi_3)(\xi_2-\xi_3)(\xi_3-\xi_4)} & -\frac{\xi_2\xi_3+\xi_1(\xi_2+\xi_3)}{(\xi_1-\xi_4)(\xi_2-\xi_4)(\xi_3-\xi_4)} \\ -\frac{\xi_2\xi_3\xi_4}{(\xi_1-\xi_2)(\xi_1-\xi_3)(\xi_1-\xi_4)} & \frac{\xi_1\xi_3\xi_4}{(\xi_1-\xi_2)(\xi_2-\xi_3)(\xi_2-\xi_4)} & -\frac{\xi_1\xi_2\xi_4}{(\xi_1-\xi_3)(\xi_2-\xi_3)(\xi_3-\xi_4)} & \frac{\xi_1\xi_2\xi_3}{(\xi_1-\xi_4)(\xi_2-\xi_4)(\xi_3-\xi_4)} \end{bmatrix} \tag{A6}$$

where ξ_n is the n-th element of the third column of $\mathbf{X}_i$ (i.e., coinciding with x_n if $n < i$ or x_{n+1} if $n \geq i$, with $n = 1, \ldots, 4$). Introducing also a vector of modal amplitudes $\mathbf{y}_{j,i}^U$ formed by all the values of modal shapes except for the i-th

$$\mathbf{y}_{j,i}^U = \left[\phi_{j,1}^U \ldots \phi_{j,i-1}^U \; \phi_{j,i+1}^U \ldots \phi_{j,5}^U\right]^T \tag{A7}$$

the missing i-th element can be written as a function of the other elements as

$$\phi_{j,i}^U = \mathbf{x}_i^T \boldsymbol{\theta}_{j,i}^U = \mathbf{x}_i^T \mathbf{X}_i^{-1} \mathbf{y}_{j,i}^U \tag{A8}$$

Moreover, an estimate of $\phi_{j,i}^U$ obtained using the spline interpolated in other locations can be calculated as

$$\hat{\phi}^U{}_{j,i} = \mathbf{x}_i^T \boldsymbol{\theta}_{j,h}^U = \mathbf{x}_i^T \mathbf{X}_h^{-1} \mathbf{y}_{j,h}^U \tag{A9}$$

where h is an index denoting a location different from i. Similarly, considering a damaged condition (D)

$$\mathbf{y}_{j,i}^D = \left[\phi_{j,1}^D \ldots \phi_{j,i-1}^D \; \phi_{j,i+1}^D \ldots \phi_{j,5}^D\right]^T \tag{A10}$$

$$\phi_{j,i}^D = \mathbf{x}_i^T \boldsymbol{\theta}_{j,i}^D = \mathbf{x}_i^T \mathbf{X}_i^{-1} \mathbf{y}_{j,i}^D \tag{A11}$$

$$\hat{\phi}^D{}_{j,i} = \mathbf{x}_i^T \boldsymbol{\theta}_{j,h}^D = \mathbf{x}_i^T \mathbf{X}_h^{-1} \mathbf{y}_{j,h}^D \tag{A12}$$

where $\boldsymbol{\theta}_{j,i}^D$ and $\mathbf{y}_{j,i}^D$ are similar to (A3) and (A7). The damage index used in this procedure is the percent variation of the interpolation error, which can be written as

$$\begin{aligned} \Delta^{\%}E_i &= 100\frac{E_{i,D} - E_{i,U}}{E_{i,U}} = 100\left(\frac{E_{i,D}}{E_{i,U}} - 1\right) \\ &= 100\left(\frac{\sqrt{\sum_{j=1}^p \left|\phi_{j,i}^D - \hat{\phi}^D{}_{j,i}\right|^2}}{\sqrt{\sum_{j=1}^p \left|\phi_{j,i}^U - \hat{\phi}^U{}_{j,i}\right|^2}} - 1\right) \end{aligned} \tag{A13}$$

In order to demonstrate that, if the number of nodes is equal to 5, i.e., if the interpolating spline is a single cubic polynomial, $\Delta^{\%}E_i$ is a constant within each subset it suffices to prove that

$$\frac{\sqrt{\sum_{j=1}^p \left|\phi_{j,i}^D - \hat{\phi}^D{}_{j,i}\right|^2}}{\sqrt{\sum_{j=1}^p \left|\phi_{j,i}^U - \hat{\phi}^U{}_{j,i}\right|^2}} = \frac{\sqrt{\sum_{j=1}^p \left|\phi_{j,h}^D - \hat{\phi}^D{}_{j,h}\right|^2}}{\sqrt{\sum_{j=1}^p \left|\phi_{j,h}^U - \hat{\phi}^U{}_{j,h}\right|^2}} \tag{A14}$$

Using the results found in (A8-A9) and (A11-A12), Eq. (A14) can be written as

$$\begin{aligned} &\frac{\sqrt{\sum_{j=1}^p \left|\mathbf{x}_i^T \mathbf{X}_i^{-1} \mathbf{y}_{j,i}^D - \mathbf{x}_i^T \mathbf{X}_h^{-1} \mathbf{y}_{j,h}^D\right|^2}}{\sqrt{\sum_{j=1}^p \left|\mathbf{x}_i^T \mathbf{X}_i^{-1} \mathbf{y}_{j,i}^U - \mathbf{x}_i^T \mathbf{X}_h^{-1} \mathbf{y}_{j,h}^U\right|^2}} \\ &= \frac{\sqrt{\sum_{j=1}^p \left|\mathbf{x}_h^T \mathbf{X}_h^{-1} \mathbf{y}_{j,h}^D - \mathbf{x}_h^T \mathbf{X}_i^{-1} \mathbf{y}_{j,i}^D\right|^2}}{\sqrt{\sum_{j=1}^p \left|\mathbf{x}_h^T \mathbf{X}_h^{-1} \mathbf{y}_{j,h}^U - \mathbf{x}_h^T \mathbf{X}_i^{-1} \mathbf{y}_{j,i}^U\right|^2}} \end{aligned} \tag{A15}$$

Using the Eqs. (A4), (A6-A7), and (A10), the terms in absolute value can be written as

$$\left|\mathbf{x}_i^T \mathbf{X}_i^{-1} \mathbf{y}_{j,i}^D - \mathbf{x}_i^T \mathbf{X}_h^{-1} \mathbf{y}_{j,h}^D\right| = \left|\mathbf{v}_i^T \boldsymbol{\Phi}_j^D\right| \tag{A16}$$

$$\left|\mathbf{x}_i^T \mathbf{X}_i^{-1} \mathbf{y}_{j,i}^U - \mathbf{x}_i^T \mathbf{X}_h^{-1} \mathbf{y}_{j,h}^U\right| = \left|\mathbf{v}_i^T \boldsymbol{\Phi}_j^U\right| \tag{A17}$$

$$\left|\mathbf{x}_h^T\mathbf{X}_i^{-1}\mathbf{y}_{j,i}^D - \mathbf{x}_h^T\mathbf{X}_h^{-1}\mathbf{y}_{j,h}^D\right| = \left|\mathbf{v}_h^T\boldsymbol{\Phi}_j^D\right| \tag{A18}$$

$$\left|\mathbf{x}_h^T\mathbf{X}_i^{-1}\mathbf{y}_{j,i}^U - \mathbf{x}_h^T\mathbf{X}_h^{-1}\mathbf{y}_{j,h}^D\right| = \left|\mathbf{v}_h^T\boldsymbol{\Phi}_j^U\right| \tag{A19}$$

It is thus possible to write Eq. (A15) as

$$\frac{\sqrt{\sum_{j=1}^{p}\left|\mathbf{v}_i^T\boldsymbol{\Phi}_j^D\right|^2}}{\sqrt{\sum_{j=1}^{p}\left|\mathbf{v}_i^T\boldsymbol{\Phi}_j^U\right|^2}} = \frac{\sqrt{\sum_{j=1}^{p}\left|\mathbf{v}_h^T\boldsymbol{\Phi}_j^D\right|^2}}{\sqrt{\sum_{j=1}^{p}\left|\mathbf{v}_h^T\boldsymbol{\Phi}_j^U\right|^2}} \tag{A20}$$

where $\boldsymbol{\Phi}_j^U$ and $\boldsymbol{\Phi}_j^D$ are the complete modal shapes in the undamaged and damaged conditions, respectively. Let the vectors $\mathbf{v}_i^T$ (and $\mathbf{v}_h^T$) have the terms different from i (or h) organized in the vector $\tilde{\mathbf{v}}_i^T$ (or $\tilde{\mathbf{v}}_h^T$, substituting h to i) with the form

$$\tilde{\mathbf{v}}_i^T = \begin{bmatrix} \frac{(x_i-\xi_2)(x_i-\xi_3)(x_i-\xi_4)}{(\xi_1-\xi_2)(\xi_1-\xi_3)(\xi_1-\xi_4)} \\ -\frac{(x_i-\xi_1)(x_i-\xi_3)(x_i-\xi_4)}{(\xi_1-\xi_2)(\xi_2-\xi_3)(\xi_2-\xi_4)} \\ \frac{(x_i-\xi_1)(x_i-\xi_2)(x_i-\xi_4)}{(\xi_1-\xi_3)(\xi_2-\xi_3)(\xi_3-\xi_4)} \\ -\frac{(x_i-\xi_1)(x_i-\xi_2)(x_i-\xi_3)}{(\xi_1-\xi_4)(\xi_2-\xi_4)(\xi_3-\xi_4)} \end{bmatrix} \tag{A21}$$

while the i-th (or h-th) term is -1. Thus, substituting any couple of values for i and h in the range from 2 to 4 into Eq. (A21), it results in $\left|\mathbf{v}_i^T\boldsymbol{\Phi}_j^D\right| = \left|\mathbf{v}_h^T\boldsymbol{\Phi}_j^D\right|$ and $\left|\mathbf{v}_i^T\boldsymbol{\Phi}_j^U\right| = \left|\mathbf{v}_h^T\boldsymbol{\Phi}_j^U\right|$. Therefore, Eq. (A20) is verified.